Journal of Structural Geology 32 (2010) 1712–1720

Contents lists available at ScienceDirect

Journal of Structural Geology

journal homepage: www.elsevier.com/locate/jsg

Porosity and particle shape changes leading to shear localization in small-displacement faults

Jafar Hadizadeh [a,*], Reza Sehhati [b,c], Terry Tullis [d]

[a] Department of Geography and Geosciences, University of Louisville, Louisville, KY, USA
[b] Department of Civil and Environmental Engineering, Washington State University, Pullman, WA, USA
[c] Berger/ABAM Engineering Inc., Federal Way, WA 98003, USA
[d] Department of Geological Sciences, Brown University, Providence, RI, USA

ARTICLE INFO

Article history:
Received 26 January 2009
Received in revised form
17 August 2010
Accepted 23 September 2010
Available online 1 October 2010

Keywords:
Shear localization
Gouge porosity
Particle shape and size
Particle size distribution

ABSTRACT

A microstructural study of shear localization in fault gouge was carried out in small-displacement faults so there would be minimum masking effects from a complex deformation history. We studied particle size, shape, and porosity changes in gouge adjacent to zones of shear localization in natural and synthetic gouges subjected to shear displacements δ, of up to 1.2 m. Scanning electron microscope images were used for estimating image porosity Φ_I, and measuring particle size of the deformed and undeformed gouges. The particle size data were used for calculating simulated porosity Φ_S from computer-generated simple fractal gouge model of each sample. Modeled microstructures contained round grains and a fractal distribution matched to that of the measured natural samples. Changes in Φ_I, Φ_S, and Φ_I/Φ_S with increasing δ were used for tracking changes in particle shape and porosity of the gouges precursory to shear localization. The Φ_I and Φ_S values for the natural and synthetic gouges converge at $\delta \sim 0.1$ m, suggesting that gouge particles adjacent to shear localization sites tend to become rounded. Porosity for such densified regions of the gouge adjacent to Y-shear zones was determined to be $<1\%$ at large displacements. In the same regions, the porosity reductions were also associated with decreased sorting coefficient and fractal dimensions $D > 2.6$. The study suggests that brittle shear localization may involve favorably-oriented micro porous pockets of gouge that result from competing changes in particle shape and particle size, which tend to affect gouge porosity in different ways.

1. Introduction

Brittle shear localization microstructures such as slip surfaces, shear bands, and cataclastic foliation are commonly found within the core of many natural fault zones. The localization process results in mechanical weakening of the fault and is often associated with the most comminuted and densified regions in fault gouge (e.g. Evans and Chester, 1995; Chester and Chester, 1998; Boullier et al., 2004; Hayman, 2006; Rawling and Goodwin, 2006; Rockwell and Ben-Zion, 2007; Tanaka et al., 2007; Brogi, 2008). Shear localization has been observed in relatively unaltered small-displacement faults with displacements typically <1 m as in most experimental faults as well as in mature natural fault zones involving a variety of alteration products. Experimental fault gouge studies have shown that ≤ 0.1 m of shear displacement results in shear localization, although microstructural changes leading to shear localization are not well understood. A number of studies of natural, experimental and computer simulated gouge deformation conclude that shear localization is primarily a particle size and particle-size distribution driven process (Dieterich, 1981; Marone and Scholz, 1989; Biegel et al., 1989; Logan et al., 1992; Gu and Wong, 1994; Billi, 2007; Keulen et al., 2007; Sammis and Ben-Zion, 2008). Experimental studies by Mandl et al. (1977), Vardoulakis (1980), Marone and Scholz (1989), Mair and Marone (1999), and Mair et al. (2002) indicate that gouge attains a critical strain or particle size distribution prior to shear localization. Mandl et al. (1977) based on experimental data, suggested that shear localizes in favorably-oriented bands of gouge that have achieved a critical PSD through confined comminution. This is possible because an increase in the proportion of fine particles in gouge, while not reducing cohesive forces, might reduce the friction. Subsequently, at a low threshold value of internal friction there will be a drastic reduction in boundary shear by development of a slip plane and growth of a shear zone. In the powder industry this

* Corresponding author.
E-mail address: hadizadeh@louisville.edu (J. Hadizadeh).

0191-8141/$ – see front matter © 2010 Elsevier Ltd. All rights reserved.
doi:10.1016/j.jsg.2010.09.010

phenomenon is attributed to rounding and size equalizing of particles which tend to reduce 'interlocking resistance' of a granular material (Lowrison, 1974). The microstructural aspects of the model described above draws support from a number of observations. Gouge deformation simulations by Morgan and Boettcher (1999) showed that a sharp drop in sliding contacts accompanied localized failure as fewer particles were involved in the zone of deformation. Mair and Marone (1999) studied the controlling effect of particle size on shear localization and noted that PSD evolution in fine and coarse gouge differed only by a shear strain γ of 3.4. They suggested that higher fracture toughness might have inhibited further comminution of fine gouge as its PSD became more uniform. Scarpelli and Wood (1982), Moore et al. (1989), Logan et al. (1992) reported the same sequence of microstructural development preceding shear localization in calcite and halite gouges. In a model presented by Shipton and Cowie (2001) a critical amount of comminution or strain was necessary for slip surface nucleation, but the slip surfaces accommodated further strain without appreciable amount of comminution. The experimental study of Marone and Scholz (1989) concluded that transition from pervasive to localized shear occurs at a critical strain or PSD in addition to the influence of gouge density.

This study attempts to provide a microstructural model for shear localization by investigating the combined effect of particle shape and particle size on porosity changes that precede shear localization in small-displacement natural and experimental faults. The effect of porosity changes on shear localization in granular material with varied particle size and PSD has been studied previously. The work of Mead (1925) and Frank (1965) shows that since in confined comminution dilatancy is suppressed, shear localization must occur in regions of gouge with least dilatancy rate. Marone and Scholz (1989) reported dilatant behavior at the onset of shear localization in their experimental quartz gouge. The actual shear localization occurred on R_1 Riedel shear bands, and the dilatancy was believed to be the result of unpacking of over consolidated gouge. Marone and Scholz (1989) noted that particles within their

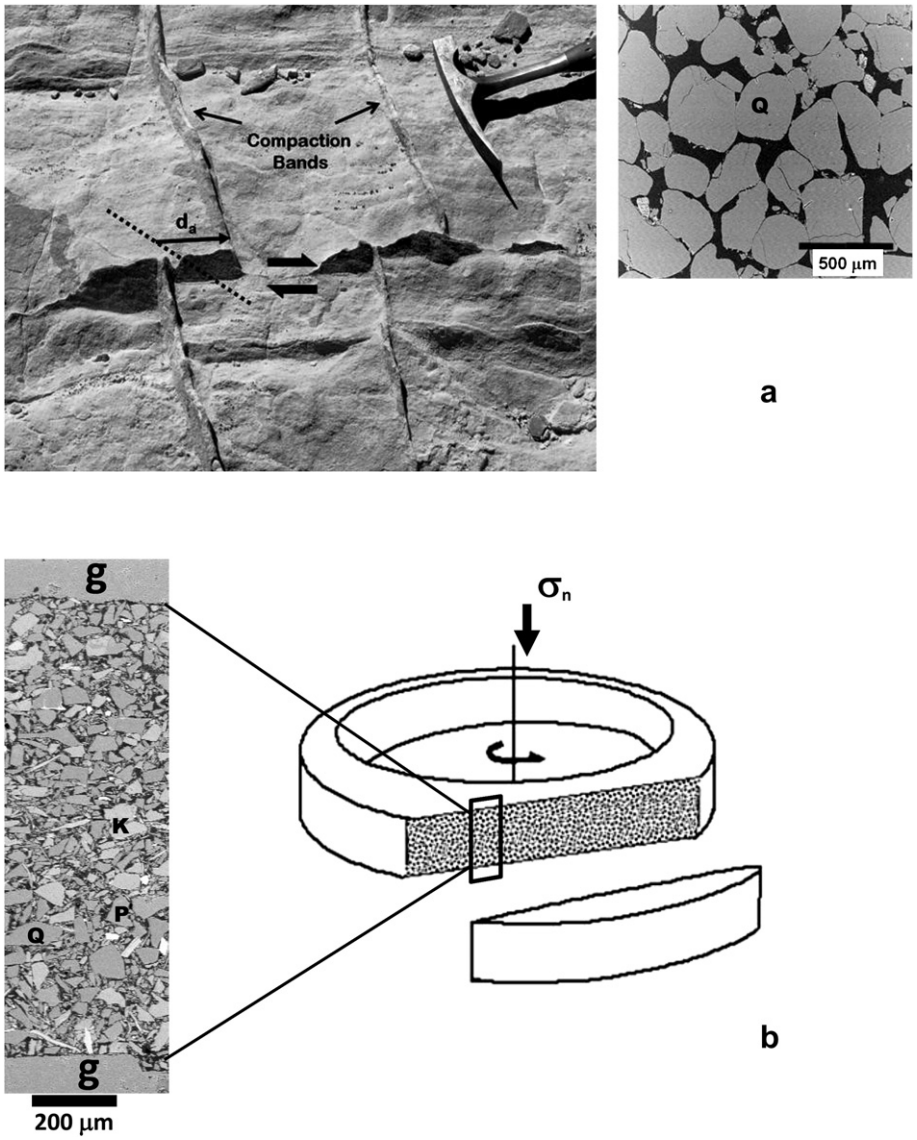

Fig. 1. Natural and synthetic gouges used in the study. (a) Typical small-displacement splay fault in the Aztec sandstone. Outcrop picture is labeled with the apparent displacement vector (d_a), and trend of the slickenside lineation on the fault plane (dotted line). Compaction bands serve as displacement markers. Typical undeformed texture of the sandstone is shown on the right. (b) Rotary shear sample ring consisting of a 2 mm gouge layer (not to scale). The close-up view of the gouge layer on the left is an actual section across undeformed simulated Westerly granite gouge compacted to 25 MPa pressure. The gouge is held between granite forcing blocks g, forming the shear zone boundaries; Q = quartz; K = potassium feldspar; P = plagioclase feldspar; lightest shade particles are phyllosilicates. Textures are back-scattered SEM images.

experimental shear bands did not follow a fractal size distribution, but the relationship between the shear band microstructures and the unpacking process was not discussed.

2. The studied fault gouges and methods of data collection

2.1. The natural gouge

Gouge samples were collected from splay faults of the Lonewolf fault zone in the Valley of Fire State Park (VOF), Nevada, U.S.A. The splay faults are believed to be sheared joints, the coalescence of which lead to the development of the Lonewolf fault zone (Flodin and Aydin, 2004; Myers and Aydin, 2004; Davatzes et al., 2003). The splay faults ranging in measurable displacement from ~0.01 m to 1.5 m were found in the upper domain of the Aztec sandstone Formation described in detail by Flodin et al. (2003). Due to soft iron oxide/clay mineral cementation of the sandstone and weathering effects, in-situ impregnation by clear resin was necessary before the samples could be lifted from the desired locations along the splay faults. The sampling method thus preserved the gouge microstructures. The Aztec sandstone in the sampling area is an aeolian feldspathic quartz arenite made of rounded to well-rounded quartz grains forming 95% of the rock with average undeformed grain size of 230 μm. The measured porosity (Flodin et al., 2003 via Helium porosimetry) ranged from 21.2% to 23.8% with the presence of a small amount of pore-filling quartz or iron oxide cement. Our sampling area corresponds to porosity samples 54–56 in Table 2, Flodin et al. (2003).

The strike-slip and normal faulting in the VOF area had taken place during the Miocene Basin and Range tectonic activity. It has been suggested that in the initial phase of the activity the Aztec Formation had been buried by at least 1.6 km of sediments (Bohannon, 1983), and possibly by an additional 1–4 km of overlying Sevier-related thrust sheet (Brock and Engelder, 1977). Based on the overburden thickness estimates and studies by Flodin and Aydin (2004) the possible range of overburden pressure at the time of faulting could be 10–40 MPa assuming an overburden density of 2700 kg/m^3. The effective pressure for the VOF gouges might have been closer to the middle of the range because for approximately same shear strains the overall degree of cataclasis in the VOF shear bands was similar to those observed in our experimental shear bands deformed at 25 MPa. We found no optical evidence of crystal plastic deformation in quartz grains of the sampled gouge, which suggested temperatures <200 °C for the observed deformation.

Compaction bands that formed prior to faulting in the Aztec sandstone (Flodin et al., 2003) were offset by the studied splay faults and provided excellent displacement markers (Fig. 1a). The measured apparent displacement d_a (the band offset), together with the pitch R of slickenside lineation on the fault plane was used to determine true displacement δ, as $d_a/\cos R$. This relationship holds for the studied faults with a strike-slip displacement component since the displacement markers (compaction bands) were oriented vertical, or near vertical (see Fig. 1a). The apparent displacement varied along the strike, but the faults were sampled exactly where the structural measurements were made. The true displacements thus calculated were 17 mm, 116 mm, 348 mm and 1219 mm for the four samples used in this study. The gouge zone thicknesses measured in thin sections at right angles to the shear zone borders ranged from 1.2 ± 0.08 mm to 15.5 ± 5 mm, positively correlating with the displacement values. A summary of the sample data is presented in Table 1.

Table 1
A summary of structural data for the studied splay faults of the Lonewolf fault zone in the Aztec sandstone.

Sample	Fault plane attitude and sense of shear	d_a, mm	R°	δ, mm	T, mm
VOF4A	284, 39NE; RL	16.5	17	17	1.2
VOF2A	340, 74SW; RI	70	53	116	1.4
VOF01	342, 72NE; LL	90	75	348	3.6
VoF5A	015, 76NW; LL	1275	17	1219	15.5

d_a = apparent displacement; $R°$ = pitch of the slickenside lineation on the fault plane; δ = true shear displacement; T = average gouge layer thickness; RL and LL respectively refer to right-lateral and left-lateral sense of shear ascertained from compaction band offset and Reidel shear sets in the fault gouge.

2.2. The synthetic gouge

Synthetic gouge samples (WGK) with particle size ≤88 μm consisting of 28% quartz, 35% microcline, 32% plagioclase, 5% mica, and <1% opaque were prepared by grinding Westerly granite. The study uses deformed synthetic gouge from a previous experimental study. The gouge had been deformed at room temperature and 25 MPa normal stress in a rotary shear apparatus. The sliding velocity was stepped between 1 μm/s (for 1 mm distance), and 10 μm/s (for 10 mm distance) in all experiments. Technical specifics of the apparatus are described elsewhere (Tullis and Weeks, 1986; Beeler et al., 1996). For each experiment approximately 1 g of the material was packed in a ring-shaped sample holder forming a ~2 mm layer of gouge with ~35% initial porosity (Fig. 1b). A compaction test showed that raising normal stress to 25 MPa at the beginning of each experiment reduces the gouge layer thickness by about 5.5% (~110 μm). The compaction run also provided references for the initial texture, PSD, and porosity. The gouge layers were deformed to 44 mm, 79 mm, and 387 mm of shear displacement. While the simulated gouge was almost entirely velocity weakening up to the largest displacements, the effect of sliding rate on shear localization was not tested.

2.3. Particle size measurements

The thin section areas selected for imaging, and the subsequent particle size and porosity measurements, were thoroughly inspected for surface damage and plucked grains. The particle size measurements other than for characterizing the undeformed materials were made on areas of gouge adjacent to zones of shear localization. It was assumed that the intensely deformed gouge within 500 μm distance either side of Y-shear zones reflect the particle shape, particle size distribution, and porosity that existed at the onset of shear localization regardless of shear strain in the samples. It has been shown that shear localization as a result of comminution occurs during the early increments (γ's 1–10) of shear strain (Marone and Scholz, 1989; Gu and Wong, 1994; Mair and Marone, 1999; Wolf et al., 2003). The minimum shear strain in VOF and WGK gouges were 14 and 22 respectively. Furthermore, we assume that as the gouge approaches the shear localization stage the regions around potential shear zone deform more intensely than in the bulk gouge. This may be so because shear localizes where gouge is weakening. Thus unlike the bulk gouge, microstructures near the localized shear zone are expected to record the process of weakening by developing a somewhat different set of textural attributes. We avoided selecting areas for microstructural measurements where relatively undeformed gouge (e.g. coarse gouge near the fault zone margins in Fig. 2a and b) was in contact with shear bands. Such contacts might indicate the possibility of shear localization due to some preexisting microstructural inhomogeneity. The PSD data sets were used in computer simulations, and for determining fractal dimension of the gouges. The measurements were conducted on polished petrographic thin sections cut perpendicular to the shear planes and viewed in back-scattered mode in a Zeiss Supra-35VP™ scanning electron microscope (SEM). Optical microscopy included transmitted and reflected

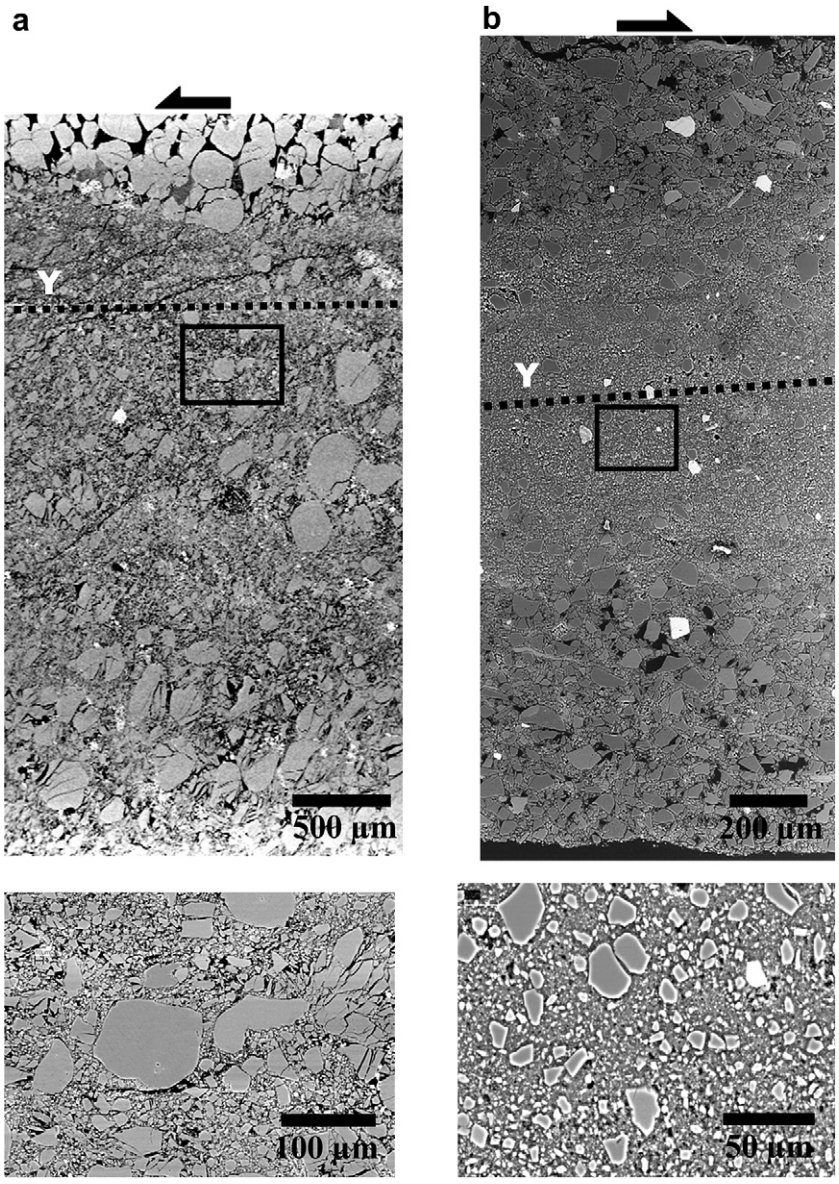

Fig. 2. Typical areas of gouge used for particle size and porosity measurements. The dotted line labeled Y is trace of the Y-shear determined from a larger area of the sample than shown here. Whole shear zones are shown on top with insets showing location of enlarged areas at the bottom. (a) Shear zone in the Aztec sandstone sample with 348 mm of displacement (VOF01 in Table 1). (b) Synthetic Westerly granite gouge layer after 44 mm of displacement (sample WGK258).

light imaging. Outline of gouge particles were manually traced on digital images from selected regions of deformed and undeformed samples. The tracing was carried out with a 2 pixel digital tip at 3× screen magnification and transformed into calibrated line drawing overlays using Adobe Photoshop™. Gouge particle size S, represented by the equivalent circle diameter of particle image area A, was measured on the overlays using relationship $S = 2(A/\pi)^{1/2}$. Measurements were carried out using SigmaScan Pro™ and MATLAB Image Processing Toolbox™ applications. To gain a wider particle size range we pooled size data for each deformed gouge sample from 2 (VOF samples) or 3 (WGK samples) sets of images taken telescopically at increasing magnification. A single SEM image each of the undeformed VOF sandstone and WGK simulated gouge was used for reference particle size measurements. In telescopic imaging, the microscope magnification was varied by a factor of two from 250× to 32000× depending on the particle size. Duplicate particle sizes (same values to 3 decimal places) in two consecutive images in each set were discarded. As mentioned earlier, particle size measurement of the deformed gouge was based on selected areas adjacent to Y-shear zones (Fig. 2). Particle size data for this study consisted of 3469 measurements (particle outline traces) acquired from 9 SEM images for the VOF samples and 5868 measurements acquired from 10 SEM images for the WGK samples. The difference in number of measurements (including the undeformed materials) reflects the smaller average particle size of the WGK gouge that resulted in a larger number of particles per unit area compared to that for the VOF gouge.

The size-number data was used for determining the fractal dimension D, as the slope of the log–log size (S) – number (N) distribution given by $N(S) = cS^{-D}$, where c is a constant (Turcotte, 1986). We present D values here as the 3D, or the volume fractal dimension by adding 1.0 to the calculated D values (Falconer, 1985).

The changes in PSD with increased shear displacement were analyzed using the sorting coefficient $Q = [S_{q1}/S_{q3}]^{1/2}$, where S_{q1} and S_{q3} are the first quartile (25% of distribution $>S_{q1}$) and the third quartile (75% of the distribution $>S_{q3}$) in a given cumulative size

distribution respectively (Krumbein and Sloss, 1951). Decreasing Q values indicate reduced particle size range, improved sorting, and increased porosity while increasing Q values indicate widening of the size range, poor sorting, and decreased porosity (Rogers and Head, 1961; Marone and Scholz, 1989). The gouge porosity here referred to as 2D image porosity Φ_I, is the total porosity estimated via digital analysis of the SEM images. Pore spaces as confirmed by secondary electron images appeared as dark featureless areas between particles on backscattered SEM images (see Fig. 1). Thus $\Phi_I = [\Sigma A_{(\text{pore space})} \times 100]/A_{(\text{image})}$, where A is the measured areas on the image. The image processing method and its validation with respect to volume porosity in actual rock material has been discussed elsewhere (e.g. Antonellini et al., 1994; Anselmatti et al., 1998; Solymar and Fabricius, 1999; Talukdar et al., 2002; Johansen et al., 2005). The sources of error in area measurements included image quality and magnification, and the thresholding process. Thresholding refers to a digital manipulation of the image that involves differentiating a certain range of pixel intensities from the full image pixel intensity distribution. For our purpose, the pore space pixel range was isolated by thresholding binarized images using SigmaScan Pro™ application. The thresholding average values were ±0.1% and ±2% of the total measured pore areas at the highest (64000×) and the lowest (250×) image magnifications respectively. After thresholding, but prior to the measurements, pore-like pixel areas within particles were removed from the threshold copy of the image. Since the particle-pore borders consisted of only a zone of 2–5 pixels, an average of the highest and lowest pore space area was used in individual images. The image porosity was then estimated by averaging Φ_I values from individual images in a telescopic series that represented each sample. A 3-image telescopic set was used for the highest displacement samples (WGK262 and VOF5A) while a 2-image telescopic set, taken at 250× and 1K×, was used in all other samples; 9 (VOF) and 7 (WGK) SEM images were used.

2.4. Porosity from computer-generated models

A computer program for generating simple fractal gouge (SFG) models was written in VC++. The basic objective of the simulations was to obtain reasonable estimates for the limiting values of porosity as gouge particles become more rounded with increased comminution. The program was not written to simulate realistic gouge microstructures; it was intended for providing estimates of porosity in a hypothetical gouge with spherical particles and fractal particle size distribution. The Φ_S values, generated based on our real gouge PSD data, were an approximation which we considered more accurate than a hypothetical PSD. The nature of the PSD approximation was that we expected a deviation to occur from the so-called steady-state fractal size distribution ($D = 2.6$) within the shear bands. The approximation is reasonable since the PSD data used for the simulations were collected from selected areas adjacent to the shear bands.

The algorithm takes as input a PSD data set acquired from gouge images as described earlier. The size and total number of particles remained unchanged from the original distribution, and the particles were simulated as perfect circles. As a fractal distribution, the particles for each simulated texture were assembled such that least number of same size particles touched. This was achieved by packing particles according to tangent circle solutions for neighboring particles. The program produced maximum packing density for the given data set under the described conditions. The packing density of the SFG models could exceed the maximum packing density achievable with uniform size circles in 2D space given by $\pi/\sqrt{12}$ (Hecht, 2004). The algorithm was capable of processing an unlimited number of particles with unlimited size range in a descending order. The 2D porosity of the SFG was calculated by summing up the void space areas within the perimeter of the entire simulated mass. Although in this study only 2D results are reported we note that the 3D porosity tends to be higher than the 2D

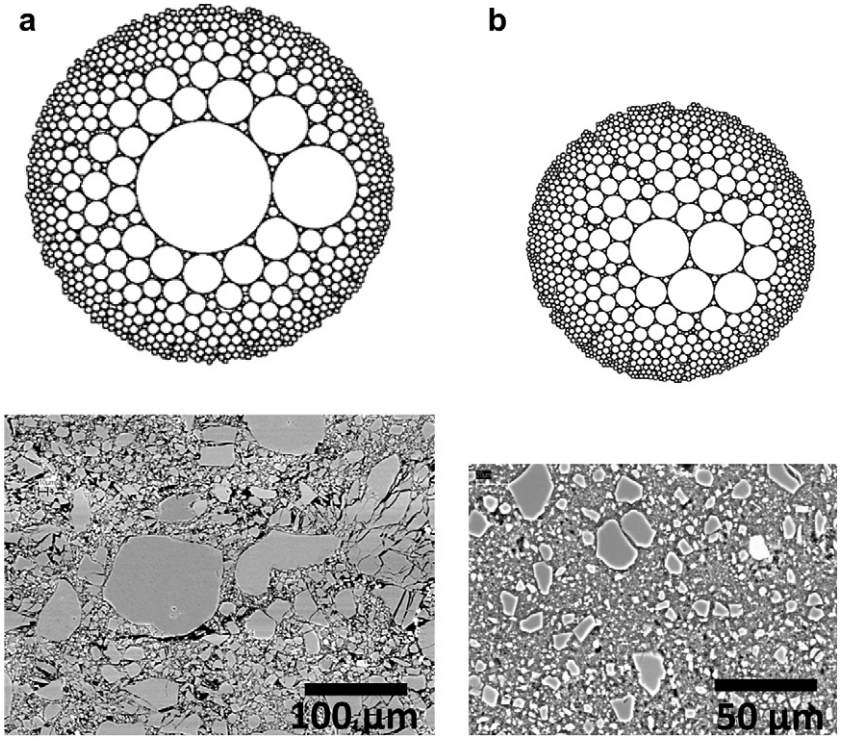

Fig. 3. Examples of the simple fractal gouge (SFG) model based on particle size data from gouge areas adjacent to Y-shear zones. Models are for (a) Aztec sandstone gouge area shown in Fig. 2a, $N = 817$ particles, $D = 3.306$, and (b) Synthetic gouge area shown in Fig. 2b, $N = 1386$ particles, $D = 3.284$. Scale bars on images are approximately true for the models.

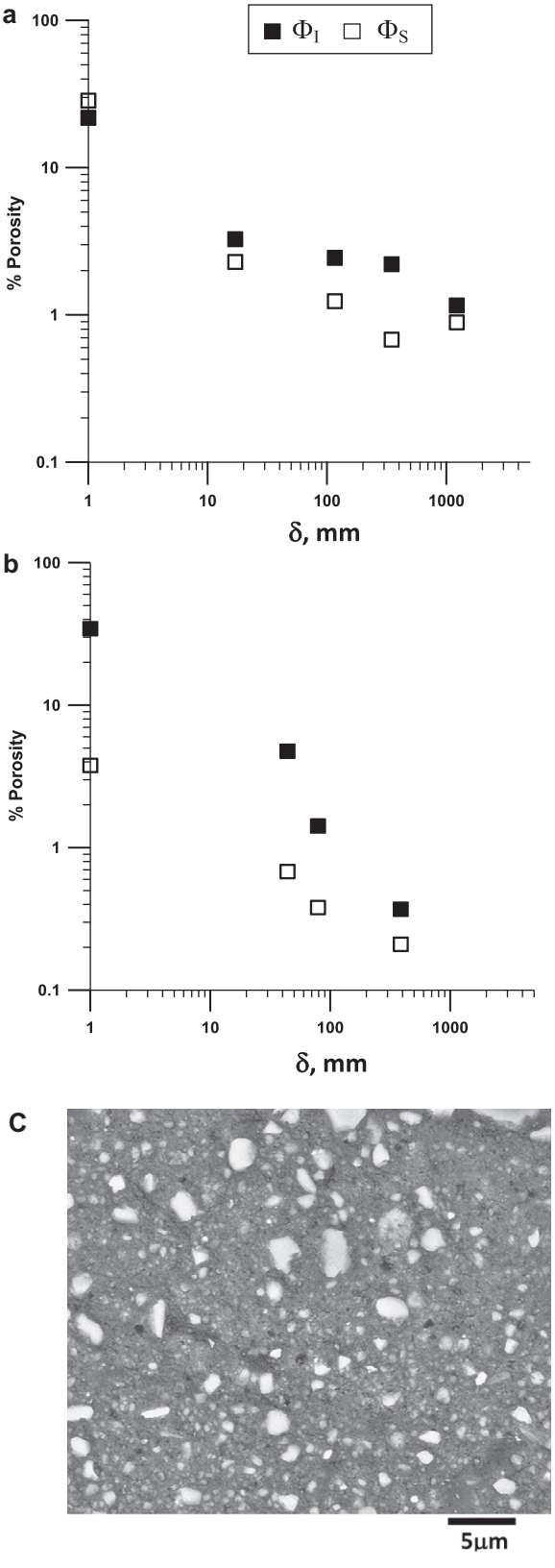

Fig. 4. Changes in porosity with shear displacement of areas adjacent to Y-shear zones in (a) The Aztec sandstone gouge and (b) Westerly granite synthetic gouge. The porosity is represented by the 2D image porosity Φ_I, and its corresponding SFG model porosity Φ_S. Undeformed gouge in both cases is assigned a nominal displacement value of 1 mm (c). SEM backscattered image of simulated Westerly granite gouge texture showing abundance of particles with round to sub rounded shapes bordering the main Y-shear zone in the experiment with 387 mm shear displacement.

porosity for the same packing arrangement. The main source of error in the simulation originated in the manual particle outline tracing operations that provided the particle size data set. This was in turn dependent upon magnification and image quality. The program numeric output included SFG porosity, Φ_S, and a simulated texture generated via a visualizer program (examples shown in Fig. 3). We note that both Φ_S and Φ_I should be considered reasonable proxies for the gouge porosity rather than actual porosity.

3. Results

The results are shown in plots of the Figs. 4–6. The measured porosity of 21–23% in the undeformed Aztec sandstone is comparable to its SFG model porosity of 28.55%. The difference is in part due to non-fractal PSD of the undeformed sandstone and the presence of pore-filling cement. In the deformed sandstone gouge, Φ_I and Φ_S values first diverge at $\delta > 20$ mm and then converge at $\delta > 300$ mm (Fig. 4a). This transient deviation from continuous porosity reduction is due to comminution of the round undeformed particles into angular particles during initial increments of shear displacement on the fault. The porosity of the sandstone gouge drops with further comminution and rounding of the cataclastic particles. For the synthetic Westerly granite gouge with initially angular particles, Φ_S and Φ_I values have their largest difference in the undeformed gouge, but the difference is reduced monotonously with increasing displacement (Fig. 4b). In terms of particle shape, Fig. 4c shows that confined comminution in the synthetic gouge results in rounding of the particles as well as size reduction, although an aggregate with initially round particles will do so by first transforming to an angular aggregate. Although in both gouge types the porosity is significantly reduced by comminution, and Φ_I and Φ_S values tend to converge at $\delta > 0.1$ m, the porosity reduction in the synthetic gouge occurs at a higher rate with respect to displacement presumably due to higher normal stresses. For example, at $\delta \sim 360$ mm Φ_I is $\sim 0.45\%$ and $\sim 1.7\%$ for the synthetic gouge and the sandstone gouge respectively. We note that as expected, $d\Phi_S/d\delta$ is nearly identical for both gouge types.

The evolution of porosity with shear displacement in the two gouge types is compared by presenting the changes as Φ_I/Φ_S ratio in

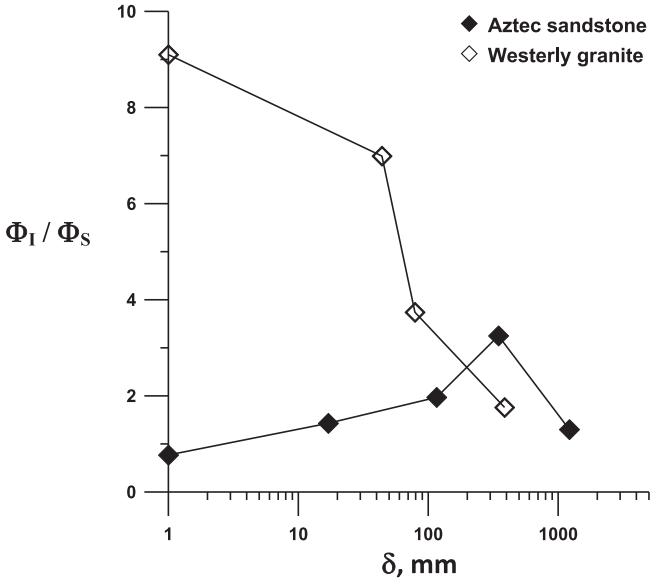

Fig. 5. Plot comparing change in Φ_I/Φ_S ratio with shear displacement in Aztec sandstone and Westerly granite synthetic gouges. The undeformed gouge is assigned a nominal displacement value of 1 mm.

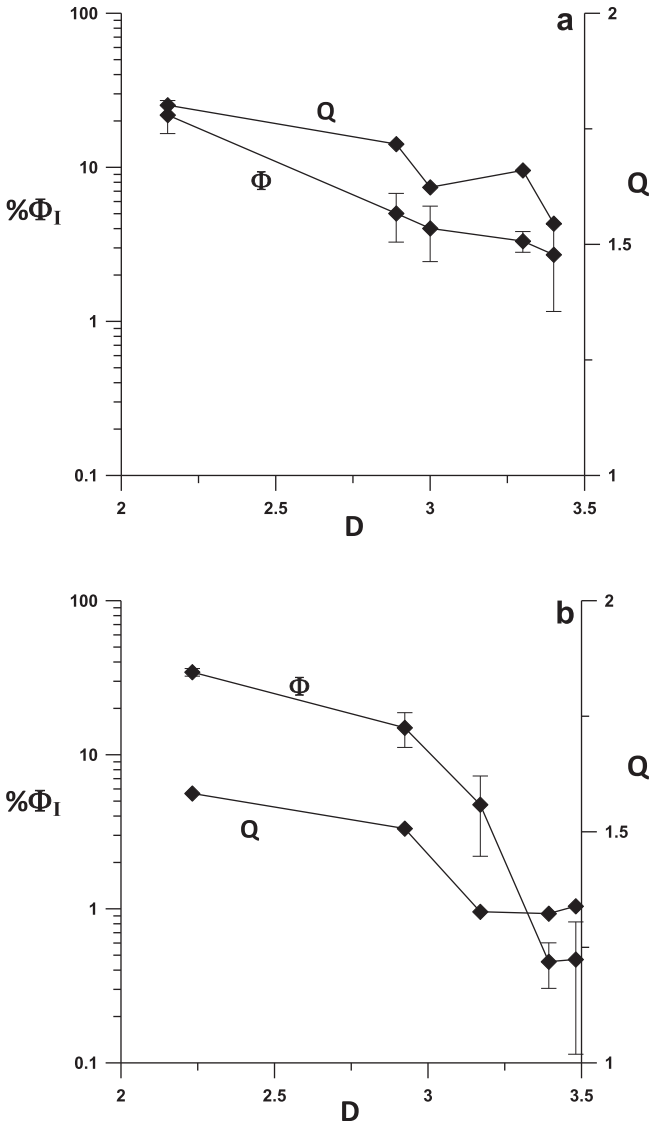

Fig. 6. Change in image porosity Φ_I and sorting ratio Q of gouge with increasing fractal dimension. Vertical error bars represent range of porosity measurements about the average. (a) Aztec sandstone gouge (b) Synthetic gouge. Higher Q values for sandstone reflect its higher average grain size compared to synthetic gouge. Data points for undeformed material are shown for reference on the left side in each case.

Fig. 5. The Φ_I/Φ_S for the two deformed gouge types converge with increasing shear displacement while remaining >1, which indicates a higher porosity for the gouges compared to their SFG models. The plots in Fig. 5 confirm that lower porosities adjacent to zones of shear localization result from rounding as well as fining of the particles. The particle shape changes are associated with increasing D values and decreasing sorting coefficient Q (decreasing size range). The interrelationship between sorting, porosity, and D, based on our data, is shown in Fig. 6. The plots indicate that densification of gouge at potential shear localization sites is concurrent with particle rounding and improved sorting.

4. Discussion

The studied gouges had not undergone appreciable hydrothermal alterations or pressure solution and lack significant phyllosilicates fractions, all of which are shown to be important factors in deformation of gouge in mature fault zones. As suggested by studies of clay–quartz gouge mixtures (e.g. Crawford et al., 2008), the microstructural and mechanical effects of phyllosilicates in quartz-feldspatic gouge are minimal if phyllosilicates make ≤5% of the gouge contents. Experimental studies also show that the process of shear localization is affected by the magnitude of the mean stress mostly in the dilatational phase (Marone and Scholz, 1989; Gu and Wong, 1994; Besuelle, 2001). This is mainly because the strain per fracture rule applicable to a fractal PSD breaks down within the shear bands (Sammis et al., 1987) and there is less number of contact points in a non-fractal aggregate. The shear localization model discussed here is relevant to microstructures within the shear bands in the post dilatational stage of the shear localization.

The results provide both visual and numeric confirmation of the correlation between shape of particles in the studied gouges and the porosity values calculated from their corresponding SFG models. The undeformed Aztec sandstone with round particles has Φ_I/Φ_S of ~1, while the undeformed synthetic Westerly granite gouge with highly angular particles has Φ_I/Φ_S of ~9. The changes in Φ_I and Φ_S values and Φ_I/Φ_S ratio with increasing shear displacement show that using the model results to infer changes in particle shape of the deformed gouges is also reasonable. In the regions adjacent to Y-shear zones, porosities calculated from SFG models change from 2% to 0.2% with increasing displacement as the corresponding gouge porosity is reduced from 5% to 0.3%. Furthermore, we showed that despite mineralogical differences of the two gouge types the microstructural attributes of the gouge adjacent to shear bands converge with increased comminution.

The particle size distribution adjacent to Y-shear zones in both gouge types consistently yields D values greater than what is considered to be an ideal gouge PSD of 2.6 produced through confined comminution (Sammis et al., 1987; Sammis and Biegel, 1989; Blenkinsop, 1991). The gouge regions with $D > 2.6$, having already achieved a high packing density, might be viewed as having a critical PSD in connection with the shear localization processes. To further define the condition we consider porosity (packing density) and sorting characteristics of the gouge from the studied regions. The sorting ratio of the gouge was shown to drop continuously with increasing displacement as the average ratio of the largest to smallest size particles within the zones was reduced from 3 to 1.3 prior to shear localization. However, to interpret the decreasing Q as an increasing porosity appears to contradict the decreasing Φ_I and Φ_S values we report in the same gouge over the same range of shear displacements. A possible explanation is that porosity reductions through particle rounding are offset by the porosity gains through decreasing Q. The SFG models clearly show that prior to shear localization the rounding effect continues with increasing shear displacement. The local dilation rate, therefore, may depend on net porosity gain or loss due to the competing effects of the changes in size and shape of particles within a densifying gouge.

A shear localization model based on the presented data and arguments above appears to be in general agreement with the localization model discussed by Marone and Scholz (1989). For shear localization in gouge with the critical PSD, a sufficient density of regions with lower dilation rate $d\Phi/d\gamma$, is required. The shear localization model illustrated in Fig. 7 thus involves unpacking (loss of cohesion at micro-scales) of densified gouge along a zone of favorably oriented pockets of relatively porous (microporous) gouge. Based on our analyses of the critical PSD above, the net porosity gain within a shear band region would occur only if the comminution process (including particle boundary attrition and transgranular fracture) becomes more effective in eliminating particle size differences than rounding the particles. The micromechanics of the competing effect could not be ascertained from this study, but the data indicates that such microstructural state is reached at fractal dimensions $D > 2.6$ as depicted in the schematic

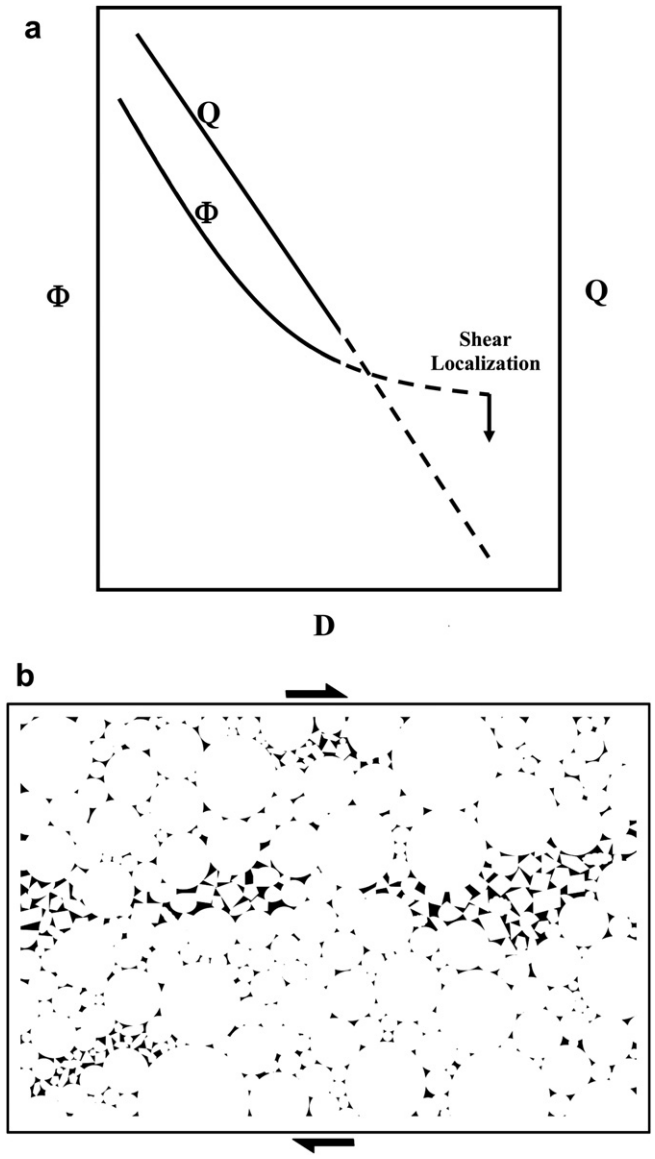

Fig. 7. A model for shear localization based on competing changes in particle shape and particle size of the gouge. (a) Behavior of microstructural variables porosity Φ, and sorting coefficient Q with increased fractal dimension of gouge shown in an ideal extrapolation of data. Shear localizes in regions of gouge where porosity increase by narrowing particle size range (decreasing Q) is greater than porosity reduction by particle rounding (decreasing Φ). Porosity is expected to drop sharply within shear localization microstructures such as shear bands. It is assumed that changes in Q and Φ take place at $D > 2.6$. (b) Highly schematic representation of gouge microstructure at the onset of shear localization in gouge (dashed line segments in a) in an approximately 20 × 15 μm area. Pockets of well-sorted porous gouge (angular particles) are bordered by dense gouge (round particles) with well distributed micro porosity. The PSD in this region of gouge has $D > 2.6$. The particle shapes are simplified and exaggerated, and sense of shear is arbitrary.

plot of Fig. 7a. It is likely, however, that shear localization in the densified gouge involves a range of D values at $D > 2.6$ rather than requiring a unique D value for the entire length of a potential shear band. This is simply because of the non-uniform nature of comminution intensity within a deforming gouge (Hadizadeh and Johnson, 2003). The model gouge microstructure at the onset of shear localization includes pockets or streaks of porous gouge, some of which are favorably oriented parallel to Y-shear orientation as illustrated in Fig. 7b. Based on a sorting criterion Marone and Scholz (1989) showed that in the bulk gouge with fractal size distribution sorting remained poor and porosity remained low since small particles tended to fill in between the larger particles. Within the bulk gouge, regions with non-fractal PSD (e.g. within shear bands) tend to have reduced particle size range, improved sorting and a higher porosity. It is assumed that regions with lower rates of porosity reduction (represented by dashed segment of porosity curve in Fig. 7a) are initially highly localized, and that these regions need not to spread throughout a significant thickness of the gouge before the unpacking occurs. This assumption is consistent with the common observation that thickness of slip surfaces and shear bands often constitute a very small fraction of the total gouge zone thickness. At particle-scale, the model is supported by previous work that shows comminution in shear localization sites tends to eliminate larger particles (Marone and Scholz, 1989; Blenkinsop, 1991; Mair and Marone, 1999) probably because the growing number of smaller particles of all shapes require larger stresses to fracture (Kendall, 1978). A uniformly distributed porosity in the densified gouge would assist the shear localization process by providing weak links between the porous pockets.

The shear strength of an incipient unpacking surface is dependent upon surface roughness (Biegel et al., 1992), which in this case is mainly determined by the maximum size and spacing of the pores in the dense gouge. Shearing of the sub-micron asperities along unpacking surfaces may explain presence of thin bands of extremely fine particles observed within shear bands and along slickenside surfaces (e.g. Yund et al., 1990; Power and Tullis, 1989).

5. Conclusions

1. Confined comminution generates similar particle shape and size distributions with increasing shear displacement in the two studied gouge types with different mineral composition and initial textures.
2. Adjacent to sites of shear localization the gouge particles are rounder and particle size range is significantly narrowed with fractal dimensions $D > 2.6$. This observation suggests that shear localization must involve unpacking of a densified gouge.
3. The microstructural data and simple fractal gouge models indicate that unpacking of the gouges might be the result of highly localized porosity variations within the densified gouge, caused by the competing effects of changes in particle shape and particle size.

Acknowledgements

We wish to thank the editors of the JSG for their valuable comments. Lori Kennedy and the anonymous reviewers of this manuscript are thanked for their constructive comments. Discussions with Judy Chester and Joseph C. White resulted in significant improvements in the manuscript. We wish to thank David Goldsby and Anoaur Koncachbaev for their assistance with the rotary shear experiments at Brown Geosciences Department, and Joseph Williams for his help with electron microscopy at the University of Louisville. This research was partially supported by the US National Science Foundation grant NSF-EAR-0229654 to Jafar Hadizadeh.

References

Antonellini, M.A., Aydin, A., et al., 1994. Microstructure of deformation bands in porous sandstones at Arches National Park, Utah. J. Struct. Geol. 16, 941–959.
Anselmatti, F.S., Luthi, S., Eberli, G.P., 1998. Quantitative characterization of carbonate pore systems by digital image analysis. AAPG Bull. 82, 1815–1836.
Beeler, N.M., Tullis, T.E., Weeks, J.D., 1996. Frictional behavior of large displacement experimental faults. J. Geophys. Res. 101, 8697–8715.
Besuelle, P., 2001. Evolution of strain localization with stress in sandstone: brittle and semi-brittle regimes. Phys. Chem. Earth (A) 26, 101–106.

Biegel, R.L., Wang, W., Scholz, C.H., Boitnott, G.N., Yoshioka, N., 1992. Micromechanics of rock friction, 1. Effects of surface roughness on initial friction and slip hardening in Westerly granite. J. Geophys. Res. 97, 8951–8964.
Biegel, R.L., Sammis, C.G., et al., 1989. The frictional properties of a simulated gouge having fractal particle distribution. J. Struct. Geol. 11, 827–846.
Billi, A., 2007. On the extent of size range and power law scaling for particles of natural carbonate fault cores. J. Struct. Geol. 29, 1512–1521.
Blenkinsop, T.G., 1991. Cataclasis and the processes of particle size reduction. PAGEOPH 136, 59–86.
Bohannon, R.G., 1983. Mesozoic and Cenozoic tectonic development of the muddy, north muddy, and northern black mountains, Clark County, Nevada. Geol. Soc. Am. Mem. 157, 125–148.
Boullier, A.-M., Fujimotob, K., Ohtanib, T., Roman-Rossa, G., Lewinc, E., Itob, H., Pezardd, P., Ildefonsed, B., 2004. Textural evidence for recent co-seismic circulation of fluids in the Nojima fault zone, Awaji Island, Japan. Tectonophys. 378, 165–181.
Brock, W.G., Engelder, T., 1977. Deformation associated with the movement of the muddy Mountain overthrust in the Buffington Windows, S. Nevada. Geol. Soc. Am. Bull. 88, 1667–1677.
Brogi, A., 2008. Fault zone architecture and permeability features in siliceous sedimentary rocks: insights from the Rapolano geothermal area (Northern Apennines, Italy). J. Struct. Geol. 30, 237–256.
Chester, F.M., Chester, J.S., 1998. Ultracataclasite structure and friction processes of the Punchbowl fault, San Andreas system, California. Tectonophys. 295, 199–221.
Crawford, B.R., Faulkner, D.R., Rutter, E.H., 2008. Strength, porosity, and permeability development during hydrostatic and shear loading of synthetic quartz–clay fault gouge. J. Geophys. Res. 113 (B03207).
Davatzes, N.C., Aydin, A., Eichhubl, P., 2003. Overprinting faulting mechanisms during the development of multiple fault sets in sandstone, Chimmney rock fault array, Utah, USA. Tectonophys. 363 (1–2), 1–18.
Dieterich, J.H., 1981. Constitutive properties of faults with simulated gouge. Mechanical behavior of crustal rocks, the Handin volume. AGU. Monog. 24, 103–120.
Evans, J.P., Chester, F.M., 1995. Fluid-rock interaction in faults of the San Andreas system: inferences from San Gabriel fault rock geochemistry and microstructures. J. Geophys. Res. 100, 13007–13020.
Falconer, K.J., 1985. Fractal Geometry: Mathematical Formulations and Applications. Cambridge University Press.
Flodin, E., Aydin, A., 2004. Evolution of a strike-slip fault network, Valley of Fire state park, southern Nevada. Geol. Soc. Am. Bull. 116, 42–59.
Flodin, E., Prasad, M., Aydin, A., 2003. Petrophysical constraints on deformation styles in Aztec sandstone, southern Nevada, USA. Pure Appl Geophys 160, 1589–1610.
Frank, F.C., 1965. On dilatancy in relation to seismic sources. Rev. Geophys. 3, 485–553.
Gu, Y., Wong, T.-F., 1994. Development of shear localization in simulated quartz gouge: effect of cumulative slip and gouge particle size. Pure Appl Geophys 143, 387–423.
Hadizadeh, J., Johnson, W.K., 2003. Estimating local strain due to comminution in experimental cataclastic textures. J. Struct. Geol. 25, 1973–1979.
Hayman, N.W., 2006. Shallow crustal fault rocks from the Black Mountain detachments, Death Valley, CA. J. Struct. Geol. 28, 1767–1784.
Hecht, C.A., 2004. Geomechanical models for clastic grain packing. Pure Appl Geophys 163, 331–349.
Johansen, T.E.S., Fossen, H., Kluge, R., 2005. The impact of syn-faulting porosity reduction on damage zone architecture in porous sandstone: an outcrop example from the Moab Fault, Utah. J. Struct. Geol. 27, 1469–1485.
Kendall, K., 1978. The impossibility of comminuting small particles by compression. Nature 272, 710–711.
Keulen, N., Heilbronner, R., Stünitz, H., Boullier, A.-M., Ito, H., 2007. Grain size distributions of fault rocks: a comparison between experimentally and naturally deformed granitoids. J. Struct. Geol. 29, 1282–1300.
Krumbein, W.C., Sloss, L.L., 1951. Stratigraphy and Sedimentation. Freeman.
Logan, J.M., Dengo, C.A., Higgs, N.G., Wang, Z.Z., 1992. Fabrics of experimental fault zones: their development and relationship to mechanical behavior. In: Fault Mechanics and Transport Properties of Rocks. Academic Press Ltd., pp. 33–66.
Lowrison, G.C., 1974. Crushing and Grinding: The Size Reduction of Solid Materials. Butterworth Publishers, London, 286 pp.
Mair, K., Marone, C., 1999. Friction of simulated fault gouge for a wide range of velocities and normal stresses. J. Geophys. Res. 104, 28899–28914.
Mair, K., Frye, K.M., et al., 2002. Influence of grain characteristics on the friction of granular shear zones. J. Geophys. Res. 107 (ECV4), 1–9.
Mandl, G., De Jong, L.N.J., Maltha, A., 1977. Shear zones in granular materials. Rock Mech. 9, 95–144.
Marone, C., Scholz, C.H., 1989. Particle-size distribution and microstructures within simulated fault gouge. J. Struct. Geol. 11, 799–814.
Mead, W.J., 1925. The geologic role of dilatancy. J. Geol. 33, 685–698.
Moore, D.E., Summers, R., et al., 1989. Sliding behavior and deformation textures of heated illite gouge. J. Struct. Geol. 11, 329–342.
Morgan, J.K., Boettcher, M.S., 1999. Numerical simulations of granular shear zones using the distinct element method 1. Shear zone kinematics and micromechanics of localization. J. Geophys. Res. 104, 2703–2719.
Myers, R., Aydin, A., 2004. The evolution of faults formed by shearing across joint zones in sandstone. J. Struct. Geol. 26, 947–966.
Power, W.L., Tullis, T.E., 1989. The relationship between slickenside surfaces in fine-grained quartz and the seismic cycle. J. Struct. Geol. 11, 879–894.
Rawling, G.C., Goodwin, L.B., 2006. Structural record of the mechanical evolution of mixed zones in faulted poorly lithified sediments, Rio Grande rift, New Mexico, USA. J. Struct. Geol. 28, 1623–1639.
Rockwell, T.K., Ben-Zion, Y., 2007. High localization of primary slip zones in large earthquakes from paleoseismic trenches: observations and implications for earthquake physics. J. Geophys. Res. 112 (B10304), 1–12.
Rogers, J.J.W., Head, W.B., 1961. Relationship between porosity, median size, and sorting coefficients of synthetic sands. J. Sediment. Petrol. 31, 467–470.
Sammis, C.G., Ben-Zion, Y., 2008. Mechanics of grain-size reduction in fault zones. J. Geophys. Res. 113.
Sammis, C.G., Biegel, R.L., 1989. Fractals, fault-gouge, and friction. Pure Appl Geophys 131, 255–271.
Sammis, C.G., King, G., Biegel, R., 1987. The kinematics of gouge deformation. Pure Appl Geophys 125, 777–812.
Scarpelli, G., Wood, D.M., 1982. Experimental observations of shear band patterns in direct shear tests. In: Vermeer, P.A., Luger, H.J. (Eds.), Deformation and Failure of Granular Materials. IUTAM Delft, Balkema, Rotterdam, Netherlands, pp. 473–484.
Shipton, Z.K., Cowie, P.A., 2001. Damage zone and slip-surface evolution over micron to km scales in high-porosity Navajo sandstone, Utah. J. Struct. Geol. 23, 1825–1844.
Solymar, M., Fabricius, I.L., 1999. Image analysis and estimation of porosity and permeability of Arnager Greensand, upper Cretaceous, Denmark. Phys. Chem. Earth (A) 24, 587–591.
Talukdar, M.S., Torsaeter, O., Ioannnidis, M.A., Howard, J.I., 2002. Stochastic reconstruction of chalk from 2D images. Transport Porous Media 48, 101–123.
Tanaka, H., Omura, K., Matsuda, T., Ikeda, R., Kobayashi, K., Murakami, M., Shimada, K., 2007. Architectural evolution of the Nojima fault and identification of the activated slip layer by Kobe earthquake. J. Geophys. Res. 112 (B07304), 1–20.
Tullis, T.E., Weeks, J.D., 1986. Constitutive behavior and stability of frictional sliding of granite. Pure Appl Geophys 124, 384–414.
Turcotte, D.L., 1986. Fractals and fragmentation. J. Geophys. Res. 91, 1921–1926.
Vardoulakis, I., 1980. Shear band inclination and shear modulus of sand in biaxial tests. Int. J. Numer. Anal. Meth. Geomech. 4, 103–119.
Wolf, H., Konig, D., et al., 2003. Experimental investigation of shear band patterns in granular material. J. Struct. Geol. 25, 1229–1240.
Yund, R.A., Blanpied, M.L., Tullis, T.E., Weeks, J.P., 1990. Amorphous material in high strain experimental fault gouges. J. Geophys. Res. 95, 15589–15602.